Renewable Energy 69 (2014) 166–173

Contents lists available at ScienceDirect

Renewable Energy

journal homepage: www.elsevier.com/locate/renene

Design optimization of micro-fabricated thermoelectric devices for solar power generation

Lobat Tayebi [a,b], Zahra Zamanipour [c], Daryoosh Vashaee [c,*]

[a] Helmerich Advanced Technology Research Center, School of Material Science and Engineering, Oklahoma State University, 526 N Elgin Ave, HRC, Tulsa, OK 74106, USA
[b] School of Chemical Engineering, Oklahoma State University, Stillwater, OK 74078, USA
[c] Helmerich Advanced Technology Research Center, School of Electrical and Computer Engineering, Oklahoma State University, 526 N Elgin Ave, HRC, Tulsa, OK 74106, USA

ARTICLE INFO

Article history:
Received 9 September 2013
Accepted 7 February 2014
Available online 9 April 2014

Keywords:
Solar energy
Thermoelectric device
Micro-fabrication
Thin films
Thermal analysis

ABSTRACT

Solar thermoelectric power generation is known as an economic way to utilize the full solar spectrum energy with less dependency on daylight and weather conditions.

Despite recent advances in the development of efficient thin film thermoelectric materials, micro-fabrication techniques for batch processing of solar thermoelectric power generators have not yet been pursued. This is mainly associated with the efficiency loss and low fabrication yield resulting from the small thickness of the thermoelectric layers. To address these issues, a planar thin film solar thermoelectric generator has been designed and optimized for micro-fabrication processing. This planar design possesses two attractive benefits. First, the length of the thermoelectric element can be flexibly optimized since it is not the same as the thickness of the deposited film. Second, deposition and patterning of both n- and p-type thermoelectric layers can be easily done using conventional micro-fabrication techniques. The application of thin film infrared reflecting coatings to enhance the efficiency was further considered. Theoretical analysis shows that the efficiency of this micro-machined solar thermoelectric device is comparable with the conventional solar cells while providing a less interruptive source of energy.

1. Introduction

Solar energy has grown into various ever-evolving technologies through the years such assolar heating, passive solar building designs, photovoltaic, and solar thermal electricity. Solar heating is perhaps the oldest one which is based on collecting heat by absorbing sunlight such as in solar hot water generation systems [1,2]. The sun's energy can also be passively used for the heating and cooling of buildings where part of the building is used to store the solar heat, or to generate air flow for cooling purposes [3]. The photovoltaic is based on electron-hole excitation by solar photon absorption to generate electric power [4,5]. Solar thermal electricity, on the other hand, being significantly more efficient than photovoltaic, uses concentrated sunlight for electric power generation using mechanical heat engines [6,7].

There have been significant progress in the development of thermoelectric (TE) materials with improved figures-of-merit in different forms of nano bulk [8–11], complex structures [9,12–14], superlattices [15–17], or low dimensional forms [18]. However, there has been much less attention given to the development of high efficiency thermoelectric devices [19–21]. Recently, there has been increasing interest in taking advantage of the thermoelectric effect to replace the mechanical engine in a solar thermal cell [22–26]. The first solar thermal cell integrated with a TE generator was suggested in 1954 by Telkes [27]. With a flat radiation absorber as illustrated in Fig. 1, efficiencies of 0.63% and 3.35% were achieved without and with a solar concentrator, respectively. This and several subsequent solar TE cells mainly suffered from low efficiency due to ambient heat convection [28–30]. It was recently shown that with an evacuated enclosure the efficiency of the conventional solar TE generator can be increased to approximately 5% [24,26]. As it will be discussed, several major non-ideal heat transfer effects exist in such conventional solar TE devices that are limiting their efficiency.

* Corresponding author. Tel.: +1 918 594 8634.
E-mail addresses: vashaee@gmail.com, daryoosh.vashaee@okstate.edu (D. Vashaee).

http://dx.doi.org/10.1016/j.renene.2014.02.055
0960-1481/

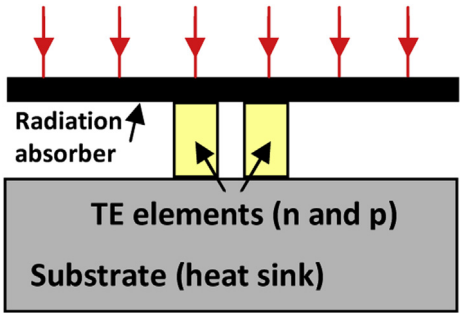

Fig. 1. Schematic of a conventional vertical solar TE device.

A solar TE device may be made either by bulk or thin film TE elements. Bulk solar TE devices, compared with the thin film design, havebeen more commonly pursued mainly due to their ease of fabrication for proof of concept demonstration and higher efficiency of the TE generator when fabricated from bulk materials [23,24,26,27,31]. However, thin film devices use significantly less material and can be manufactured with conventional micro-fabrication techniques [17,32,33]. Therefore, they are more cost effective for large-scale production. In addition, their smaller weight would reduce the cost of assembly and installation in the field. However, TE devices require significantly thicker films than typical electronic devices to work efficiently, which is difficult and costly to achieve using the conventional vacuum deposition techniques [34,35].

Micro-fabrication techniques for batch processing of thermoelectric devices have primarily suffered from low fabrication yield and poor metal contact that have road blocked thermoelectric applications such as solar power generation. In particular, thin film TE device structures suffer from several technical issues that would require their re-design for solar TE application. In brief, there are two efficiency limiting factors in a thin film TE device. The first limitation is related to the high conductivity of most TE materials, which makes the device sensitive to the contact resistances. The ohmic contact resistance (R_{oc}) must be small compared to the resistance of the TE element (R_{TE}), i.e. $R_{oc} \ll R_{TE}$ [36,37]. This condition dictates $l \gg \rho_{oc}/\rho_{TE}$, in which l is the length of the TE device, ρ_{oc} is the specific ohmic contact resistance, and ρ_{TE} is the resistivity of the TE material. Since TE materials are usually highly doped to degenerate level, ρ_{TE} is small typically in the range of $\rho_{TE} < 10^{-3}\,\Omega\,\mathrm{cm}$. For a typical contact resistance of $10^{-6}\,\Omega\,\mathrm{cm}^2$ [36], this requires $l \gg 10\,\mu\mathrm{m}$. Therefore, thin films in the range of 100 μm thick are desired to make efficient TE devices [34]. Growing such thick films with vacuum deposition techniques is often very expensive and time consuming.

The second limitation is related to the required large temperature difference ΔT between the hot side and cold side of the device. This condition results from solving the heat transfer equations for a solar TE device [38]. One can increase the ΔT by increasing the thermal resistance of the TE device and/or increasing the incoming thermal energy. To increase the thermal resistance for a given TE material, a large length to cross-section area, l/A, is desired, in which A is the cross-section area of the TE element.

To increase the incoming thermal energy, one may (a) increase A, or (b) use a large radiation absorber connected to the TE element, or (c) use a concentrator to focus the solar insolation on the TE device. (a) Is not wanted as it would decrease the l/A and reduce the ΔT. However, (b) or (c) can both be adopted for optimizing a solar TE device. We will discuss the methods based on (b) and (c) in this manuscript.

To increase the length l in a conventional vertical TE device, one has to grow thick films. However, thick film growth in the range of 100 μm has many technical barriers and is too expensive to make a viable technology. We introduce and discuss an alternative approach based on planar TE device structure to overcome the requirement for growing thick films. The design rules followed in this study are universal and can be flexibly applied to other applications with a variety of thin film thermoelectric materials utilized in similar structural designs.

2. Methodology and analytical calculations

2.1. Device configuration

The energy balance in a solar thermoelectric convertor is schematically shown in Fig. 2. The efficiency of the energy conversion can be roughly divided into the product of two terms:

$$\eta = \eta_{SA}(T_S, T_H)\eta_{TE}(T_H, T_C)$$

The first term η_{SA} is the thermal efficiency that measures the effectiveness of solar photons (with characteristic temperature at the surface of the sun T_s) in raising the temperature of the hot junction (T_H) of the devices. Obviously all mechanisms of heat losses from the solar collector or from the thermoelectric devices to the ambient and the cold side of the cell will reduce this term. The second term η_{TE} is the efficiency of the thermoelectric device when the hot and cold junction temperatures are T_H and T_c, respectively. The theoretical energy conversion efficiency η_{TE} of a thermoelectric device depends on the material figure-of-merit (ZT), and is given by:

$$\eta_{TE} = \left(1 - \frac{T_C}{T_H}\right) \frac{\sqrt{1+ZT} - 1}{\sqrt{1+ZT} + T_C/T_H} \tag{2}$$

where $ZT = S^2\sigma/\kappa \cdot T$

Here S is the Seebeck coefficient, σ is electrical conductivity, and κ is the thermal conductivity of the material. T is the average temperature. The thermal efficiency depends on various heat loss mechanisms, particularly the radiation and convection losses from the surfaces of the solar thermal collector and of the TE elements. Efficient solar TE energy conversion requires significant reduction in both heat loss sources as the efficiency increases with the temperature gradient between the two junctions.

In order to reduce the parasitic heat losses through convection, which reduces the temperature gradient, operation of the device in a vacuum package that encapsulates the module is necessary. In order to reduce radiation heat losses, the thermal collector and the cold surface of the device are coated with spectrally selective materials. In this configuration, solar energy is absorbed by a spectrally selective surface that has a high absorptivity to solar spectrum but a low emissivity at its temperature of operation. The cold side of the

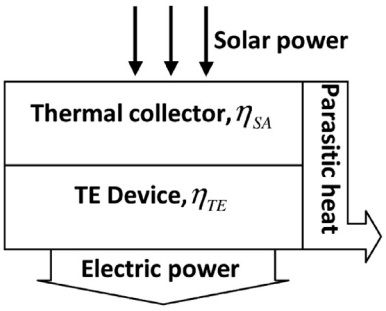

Fig. 2. Schematic of energy balance in a solar TE convector.

TE element is also coated with highly reflective surface at infrared and near infrared spectrum. In order to enhance the energy conversion efficiency, the direction here is to increase the temperature gradient across the device. In such a configuration the absorbed heat is enforced to create a large temperature gradient across the TE elements.

2.2. Efficiency of the solar TE generator

In order to address the technological barriers in making high efficiency solar TE devices in the conventional design, we considered a vertical solar TE module. It consists of one n-type and one p-type TE leg, which are electrically in series and thermally in parallel. The configuration can be different, but it does not change the basic arguments. Also, for simplicity we assume that the legs have similar electrical (σ) and thermal (κ) conductivities. The Seebeck coefficient for the n-type leg is S_n and for the p-type leg is S_p. The efficiency of this solar-driven TE generator can be written as:

$$\eta = \frac{\text{Output electric power}}{\text{Input solar power}} = \frac{IS_{np}(T_H - T_C) - 2I^2R}{A_{col}q_{solar}} \tag{3}$$

where I is the current, and $S_{np} = S_p - S_n$. $R = (1/\sigma)(l/A_{TE})$ is the resistance of the TE leg, where l and A_{Te} are the length and cross-section area of the TE legs, respectively. A_{col} is the collector surface area, and q_s is the solar power per unit area. Our goal is to optimize the device for maximum efficiency. Fig. 3 shows the energy balance in this solar TE cell. The energy balance at equilibrium with collector plate as the control volume is:

$$\frac{dE}{dt} = Q_{in} + Q_{ref2} + Q_{ref3} - Q_{ra} - Q_{rc} - Q_p - Q_c + Q_j + Q_{oc} = 0 \tag{4}$$

The incoming radiation is the solar radiation q_{solar} multiplied by the transmissivity of the cap τ_g and by the absorption coefficient of the collector α_{col}: i.e. $Q_{in} = A_{col}\tau_g\alpha_{col}q_{solar}$.

The reradiated heat from the upper surface of the collector to the ambient Q_{ra} and from its lower surface to the substrate Q_{rc} is given by:

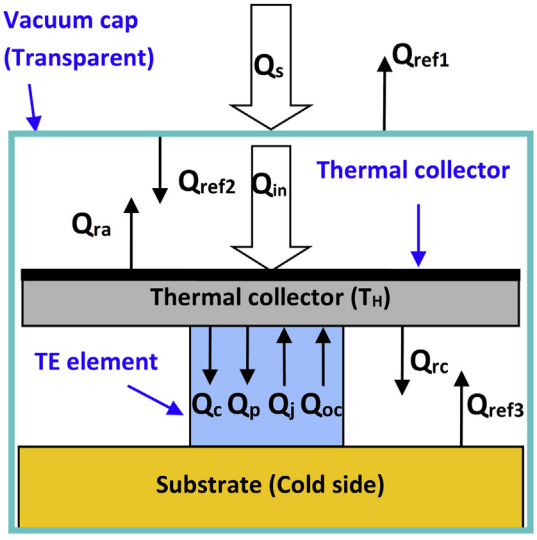

Fig. 3. Schematic of the energy balance in a vertical solar TE cell. Q_s: solar energy, Q_{ref1}: reflection from the cell to ambient, Q_{ref2}: reflection from the cell to the collector, Q_{ref3}: reflection from the cold surface, and Q_{ra}: radiation heat to ambient.

$$Q_{ra} = Q^0_{ra}/(1 - r_{cell}r_1) \text{ and } Q_{rc} = Q^0_{rc}/(1 - r_s r_2) \tag{5}$$

where $Q^0_{ra} = A_{col}\varepsilon_1\sigma(T_H^4 - T_{amb}^4)$ and $Q^0_{rc} = A_{col}\varepsilon_2\sigma(T_H^4 - T_c^4)$. The reflected heat from the cell Q_{ref2} and the substrate Q_{ref3} is given by:

$$Q_{ref2} = Q^0_{ra}r_{cell}/(1 - r_{cell}r_1) \text{ and } Q_{ref3} = Q^0_{rc}r_s/(1 - r_s r_2) \tag{6}$$

Here, r_{cell}, r_s, r_1, and r_2 are the reflectivity of the cell, substrate, collector top surface, and collector bottom surface for the incident thermal energy, respectively. ε_1 and ε_1 are the emissivity of the top and bottom sides of the collector, respectively. Q_c is the heat conduction through the TE legs, which includes both the joule heating and the conduction from the hot side to the cold side:

$$Q_c = 2\frac{\kappa A_{TE}}{l}(T_H - T_C) - I^2\frac{l}{\sigma A_{TE}} \tag{7}$$

Q_p is the Peltier heat that can be estimated by $Q_p = 2I(S_p - S_n)T_H$. Q_j is the joule heating of the TE legs, and Q_{oc} is the joule heating of the contact resistance estimated by $Q_{oc} = \rho_{oc}/A_{TE}$. Therefore, the energy balance equation can be written as:

$$\begin{aligned} g(I,T_H,A_{TE}) \equiv & A_{col}\tau_g\alpha_{col}q_{solar} - A_{col}\varepsilon_1\sigma\left(T_H^4 - T_{amb}^4\right) \\ & \times(1-r_{cell})/(1-r_{cell}r_1) - A_{col}\varepsilon_2\sigma\times\left(T_H^4 - T_c^4\right) \\ & \times(1-r_s)/(1-r_s r_2) - 2I(S_p - S_n)T_H - 2\frac{\kappa A_{TE}}{l}(T_H - T_C) \\ & + I^2\frac{l}{\sigma A_{TE}} + \frac{\rho_{oc}}{A_{TE}} = 0 \end{aligned} \tag{8}$$

where g is the Lagrange multiplier, ρ_{oc} (Ωcm^2) is the ohmic contact resistance. In order to maximize the cell efficiency given by Eq. (3), we used the Lagrange multiplier method with Eq. (8) as the constraint. Numerical solutions of the resulting equations will give us the optimum values of the current I, hot side temperature T_H, and the collector area A_{TE}. We have ignored the thermal radiation from the TE legs due to their small surface area. We have also ignored the blocking of the substrate or the collector radiations by the TE legs for a similar reason. We intend to estimate attainable efficiency with the assumption that the cell is made of the commonly available materials. We have verified this model for a vertical configuration as in Fig. 1 and compared it with Telkes's [27] and Lidorenko's [29] experimental data. We assume that the TE material used in that cell has a realistic ZT of one with $S_n = -210$ μV/K and $S_p = 220$ μV/K that correspond to typical values for Bi2Te3 based thermoelectric alloys. The solar radiation is assumed to be the standard value of 1000 W/m^2 which is typical value for a sunny day in the summer time. The cold side temperature is assumed to be fixed at 300 K.

The result is shown in Fig. 4. The absorption and emission coefficients of the high absorptive and low emitting thermal collector surface are assumed to be 0.95 and 0.05, respectively, in accordance to many available materials for this purpose. As for the ohmic contact resistance, we assumed a practical value of $10^{-6}\,\Omega\,cm^2$. The cell is made of glass with $\tau_{cell} = 0.9$, and a copper thermal collector with high absorption coating on the top surface with $\alpha = 0.95$. The emissivity of the substrate and both sides of the collector are assumed to be ~0.03 (i.e. $\varepsilon_1 = \varepsilon_2 = \varepsilon_3 = 0.03$). In this device, the thermal reflection from all surfaces is negligible and ignored in the calculations. A maximum efficiency of 3.9% is predicted for this device when the cross-section area of the TE leg is about 2.2 mm. This predicted optimum efficiency is in agreement with the order of the measurements by Lidorenko (i.e. 3.7%). It is seen that there is an optimum size for the cross-section area of the TE leg. A small cross-

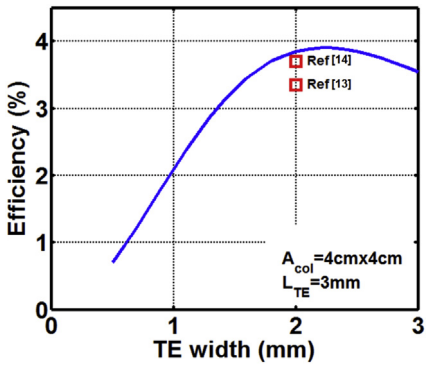

Fig. 4. Model calculation for the optimum efficiency of a conventional solar TE cell (Fig. 1). The experimental data of two devices are shown for comparison.

section area would increase the temperature, hence the radiation loss. On the other hand, a larger cross-section area would increase the thermal conduction between the hot and cold side resulting in smaller ΔT (i.e. $T_H - T_C$), which in turn would reduce the efficiency. That explains that there is an optimum size for the TE leg. Here we have assumed one TE element, where a TE element is made from two TE legs, one n-type and one p-type. Increasing the number of TE elements has same result as increasing the cross-section area.

The efficiency as shown in Fig. 4 is obviously too small to be of significant practical use compared to the state-of-the-art PV cells. It will be discussed in the following sections how the efficiency can be increased by modifying the device structure.

2.3. Vertical structure – chip scale challenges

For chip scale batch processing of the solar TE unit cells one would desire to scale down the sizes to micro-scale. However, as discussed before, reducing the size introduces new complexities in terms of contact resistance and the aspect ratio (l/A) that can further limit the efficiency. This is also the main reason for low efficiency of the solar thermoelectric generators based on bulk thermoelectrics as the device mechanical integrity dictates a limit for maximum l/A [24,26].

2.3.1. Ohmic contact resistance

In order to demonstrate the effect of Ohmic contact resistance, we considered a similar structure as in Fig. 1, but scaled down the sizes to micro-scale. The result is shown in Fig. 5. A significant drop in efficiency is observed with maximum efficiency of only ~1.4% for the micro-scale device. This is mainly due to the ohmic contact resistance between the metal contact and the TE device. We assumed a typical value of $10^{-6}\,\Omega\,cm^2$ for the ohmic contact resistance. It is generally true that most thin film TE devices suffer from the energy loss due to the ohmic contact resistance [37]. This is because TE materials are often highly doped resulting in their small electrical resistivity compared with conventional electronic materials. While the resistance of the TE device reduces with its length, the ohmic contact resistance is not a function of the length. In a TE thin film where the thickness is a few microns, the electrical resistance of the TE device can be comparable to (or even smaller than) the ohmic contact resistance. Hence, the energy loss in the contact is comparable to (or larger than) the loss in the TE material, which can limit the efficiency.

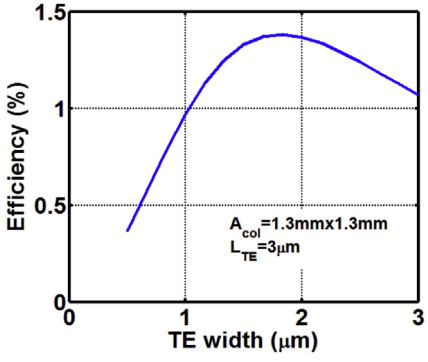

Fig. 5. Model calculation for the optimum efficiency of a micro-scale version of the conventional solar TE cell shown in Fig. 4.

2.3.2. Large aspect ratio

While it is possible to scale every size down to micro-scale, the thin film often has a maximum practical thickness (i.e. approximately a few microns) as it is rather expensive or impractical to grow tens of microns of TE film with vacuum deposition techniques. For a practical 3μm thick film, the optimum TE size is about 1.8 μm × 1.8 μm for the given collector area of 1.3 mm × 1.3 mm. One obvious shortcoming is that the aspect ratio is rather large (A_{col}/A_{TE} ~5×10^5). A smaller collector area results in smaller temperature difference for a given solar power that would reduce the efficiency. Therefore, the relative size of the collector area and the cross-section area of the TE leg sets the efficiency for the given material properties and solar power.

Therefore, the large ohmic contact resistance and the aspect ratio set a limitation on the efficiency of a vertical micro-scale solar TE cell. In the following, we design a planar cell that allows for this limitation to be resolved. We will also discuss methods to further enhance the efficiency.

3. Planar design for solar TE cell

In our design for a planar solar TE cell, unlike the majority of the TE converters, the hot junction is in the same plane as the cold junction. Fig. 6a and b demonstrates two configurations of this cell with two different approaches to increase ΔT across a TE element. In Fig. 6(a1) and (a2) a radiation absorber platform is raised above the surface of the substrate in an attempt to maximize the fill-factor. In Fig. 6(b1) and (b2) a Fresnel lens is used to concentrate the IR radiation on the TE hot junction. We will discuss the first design in detail in the next section and leave out the second design for future studies. Both methods would improve the ΔT across the TE elements. In such designs the incident radiation will mostly be absorbed by the absorbing area, which is the hot junction of the TE device, without the electrical connections receiving the radiation. In the first design, Fig. 6a, the IR absorber is made of materials with high thermal conductivity, low density, high IR absorption coefficient and small thickness (~1 μm). The absorber is connected to the TE junction which is the hot side of the device. If the cross-section area of TE elements is too small to support the weight of the absorber, the void region under the TE elements can be filled with an insulating material. A good insulating material is Parylene for its ultra-small thermal conductivity (~0.08 W/mK) and chemical stability up to 350 °C [39]. Several TE arms connect the hot junction to the cold junction. The number of TE arms placed in series can be optimized versus the electrical and thermal material properties. To further enhance the efficiency, the arms are turned around the suspended membrane to create a longer path and consequently to lower the thermal conductance while spanning over a small area, which would increase the ΔT across the TE element. This way the device can be reduced in size, resulting in a

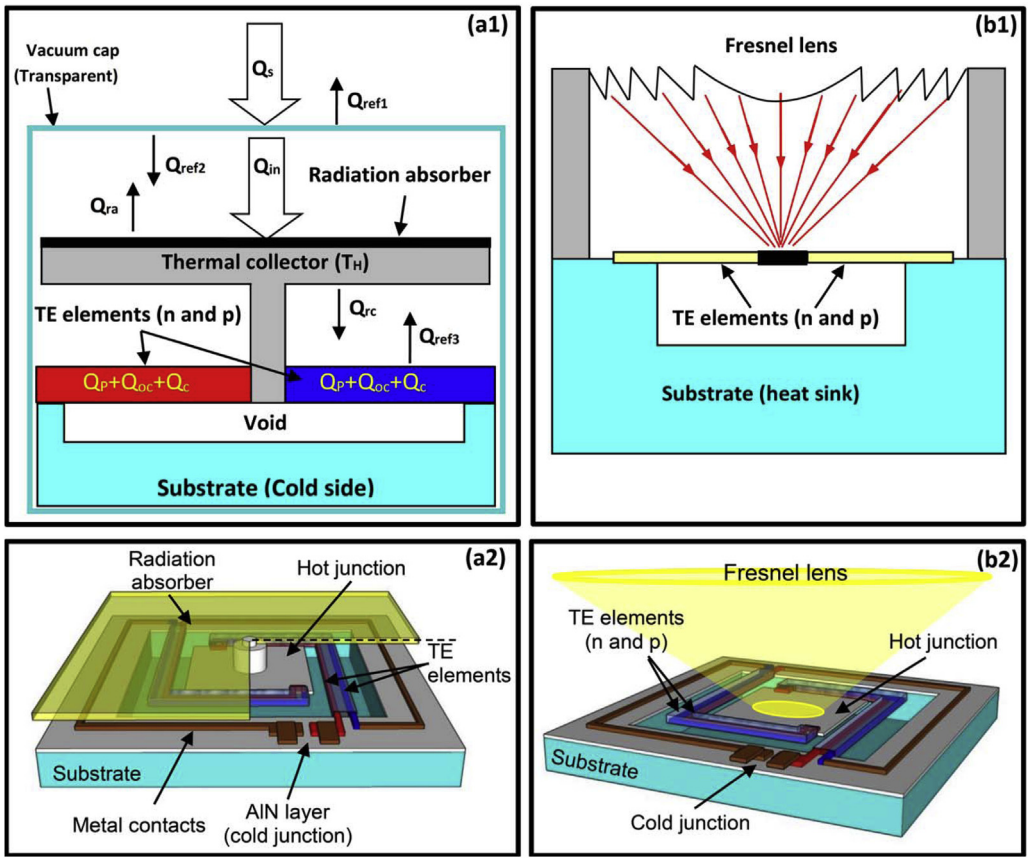

Fig. 6. (a1) and (a2) Schematic of the planar solar TE device with a thermal collector. The energy balance is also shown with Q_s: solar energy, Q_{ref1}: reflection from the cell to ambient, Q_{ref2}: reflection from the cell to the collector, Q_{ref3}: reflection from the cold surface, Q_{ra}: radiation heat to ambient, Q_{rc}: radiation heat to the cold surface, Q_p: Peltier heat, Q_c: conducted heat, Q_{oc}: ohmic contact joule heat. (b1) and (b2) Schematic of the planar solar TE with a concentrator.

smaller overall package and a lower cost while maintaining a large temperature gradient for enhanced efficiency.

This planar design possesses several attractive features: First, unlike the vertical design where the length of the TE element is equal to the thickness of the film [27,28], the TE element length in the planar design can be flexibly varied independent from the thickness. This feature is especially important in thin film thermoelectric devices where increasing the thickness of the film is usually impractical beyond a relatively small value (few micrometers). This design allows forming the TE element with virtually no limit on the length. For example lengths of several 100μm are achievable (as opposed to a vertical design that is practically limited to a few microns). This will significantly reduce the deteriorating effect of the ohmic contact resistance on efficiency. Hence, this cell offers similar efficiencies as in Fig. 4; moreover, it would result in a more practical aspect ratio (e.g. $A_{col}/A_{TE} \sim 1500$ for 300 μm long TE leg). Such a large aspect ratio is not practically achievable in solar thermoelectric generators based on bulk structures [26].

Second, deposition and patterning of both n- and p-type TE layers can be easily done using conventional fabrication or printing techniques since the TE layers are thin and patterning of one layer would not disrupt the next patterning step.

3.1. Spectrally selective coatings

In order to improve the efficiency of the planar TE cell beyond the levels achievable through implementing planar TE legs, the properties of spectrally selective coatings in this cell can be utilized.

As discussed, ideally one would like the solar radiation to be exclusively absorbed on the collector and the heat to only be conducted through the TE device. Any other thermal path is unfavorable and would reduce the efficiency [37]. The vacuum encapsulation reduces the convection losses from the collector. When the cell is evacuated, the energy from the collector is lost mainly through radiation either to the ambient or to the substrate. To further reduce these losses, the transparent cap and the substrate can be coated with spectrally selective coatings which reflect the thermal radiation. In addition, the coating material used on the cap has to be transparent to the solar spectral range. There have been great advances in window technology to substantially reduce thermal radiation losses [40]. Today, many windows are manufactured with glasses which carry spectrally selective coatings that transmit solar radiation and reflect the outgoing thermal radiation. Such coatings greatly reduce the heat losses through radiation, which account for two-thirds of heat transfer through a double-glazed window. The coatings have a high reflectance in the thermal infrared (IR) spectrum and a high transmittance to the solar photons. Most coatings are either (1) a material with the desired intrinsic properties such as doped oxides of tin or indium, which are wide bandgap semiconductors and by adjusting the dopant level, one can tune the cutoff wavelength between transmittance and reflectance, or (2) a combination of several materials such as thin films of nobel metals, especially silver, to achieve the desired performance. These coatings can be made highly transparent to visible radiation, but remain reflective in the thermal range.

We now consider the planar micro-scale cell as shown in Fig. 6 and apply the spectrally selective coatings on the inner surface of the vacuum caps. No concentrator is used and the new configuration is modeled while all the properties are kept the same as before (previous section) and only a single layer silver coating on the

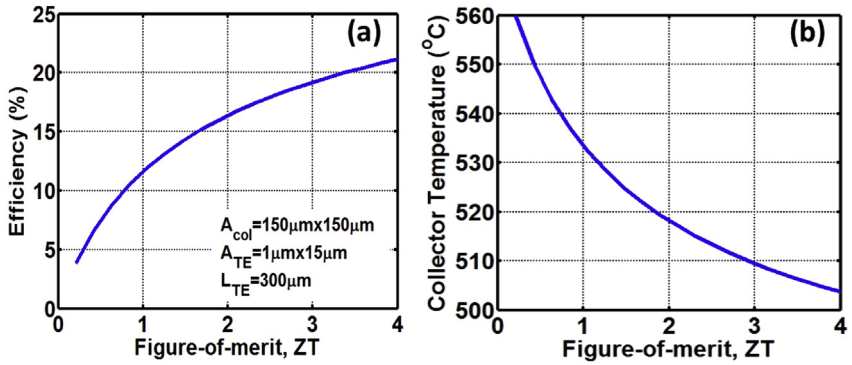

Fig. 7. (a) The efficiency and (b) the collector temperature of the proposed planar solar TE cell versus figure-of-merit, ZT. Standard solar insolation of 1000 W/m^2 is assumed.

transparent cap and a double metal layer coating on the substrate are considered. We assume the following values for the optical properties of these layers, which are extracted from the experimental data in the literature [37]:

(1) The transmission coefficient of the cell cap $\tau_{cell} = 0.83$;
(2) The thermal energy reflectivity of the cap coating $r_{cell} = 0.85$; and
(3) The thermal energy reflectivity of the substrate coating $r_s = 0.95$.

Here the high temperature selective surface of Co-Al_2O_3 is considered for the thermal collector. The absorption coefficient, α_{col} and emissivity, ε of the collector are updated with $\alpha_{col} = 0.94$ and $\varepsilon_1 = \varepsilon_1 = 0.04$ which correspond to those of Co-Al_2O_3appropriate for high temperature applications ($T \sim 500$ °C) [41].

Our model calculations show that the efficiency of the proposed solar TE cell is significantly enhanced as shown in Fig. 7a. A cell efficiency of about 12.6% is predicted even for the ZT of one. There are three TE elements electrically in series and thermally in parallel in this device. Each element consists of one n- and one p-type TE leg making a junction at the thermal collector. The collector surface area is chosen to be 150 μm × 150 μm in order to obtain a reasonable size for the two TE legs. We assumed thermoelectric properties close to those of PbTe alloys, i.e. $S = 200$ μV/K, $\kappa = 1.5$ W/mK and $\sigma = 470$ S/cm at ZT = 1 for both n- and p-types. For other values of ZT, the electrical conductivity was changed accordingly while keeping the other parameters constant. The optimum size of each TE leg for this cell is 1 μm (H) × 15 μm (W) × 300 μm (L). If we use a different collector size, the optimum cross-section area of the TE leg would be different, but the maximum attainable efficiency is not affected. The efficiency of the proposed solar TE energy conversion can be further improved by using more efficient TE materials as they become commercially available. A conversion efficiency of over 20% can be realized assuming availability of TE material with $ZT \sim 3$. The main reason for achieving such enhancement in the efficiency is due to (1) the better thermal management that the proposed structure offers resulting in large temperature gradient across the TE leg ($\Delta T > 500$ °C) as shown in Fig. 7b, and (2) reducing the effect of the ohmic contact resistance by making long TE devices in a planar structure.

3.2. Finite element analysis

In order to confirm the results of the one-dimensional analytical models, we have solved the heat transfer equation for the three-dimensional structure using finite element method in COMSOL. Heat conduction in all segments and radiation from and to all the surfaces are considered in this analysis. The solution for the temperature distribution in the structure is shown in Fig. 8. It was observed that for a 1000 W/m^2 and 400 W/m^2 solar radiation, temperature differences of approximately 474 °C and 315 °C exist across the TE legs, respectively. Fig. 9 shows the calculated temperature difference versus the solar radiation power density. It is observed that the temperature difference increases rapidly at lower solar radiation and the rate of increase reduces as the solar radiation, hence the temperature, increases. This can be associated with the increase of the radiation loss as the temperature increases. While we had ignored the radiation loss from the thermoelectric elements in the one-dimensional study presented in the previous section, in the finite element analysis the radiation loss is taken into account from all the surfaces including the thermoelectric

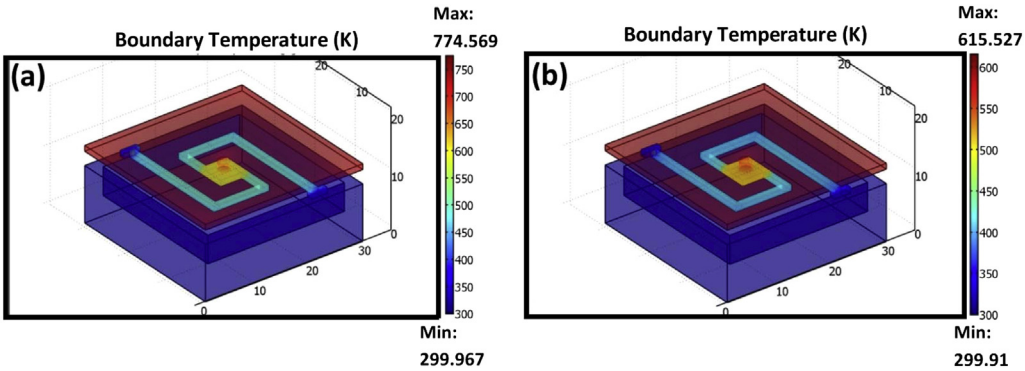

Fig. 8. The simulated temperature distribution when the collector is receiving (a) 1000 W/m^2 and (b) 400 W/m^{2}solar radiation. The simulation confirms that the $\Delta T \sim 475$ °C and 315 °C are achievable, respectively.

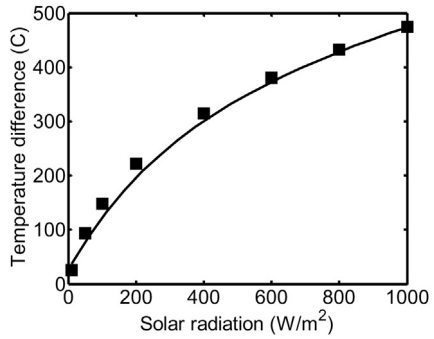

Fig. 9. Three-dimensional finite element analysis of the temperature difference (symbols) versus solar radiation power density. Solid line shows the data from one-dimensional analysis.

elements. This can explain the small temperature difference calculated from the finite element analysis compared with the one-dimensional method.

3.3. Efficiency in different weather conditions

Part of the solar radiation entering the earth's surface is absorbed, reflected, or scattered by the earth's atmosphere and the clouds. Therefore, part of the global radiation on the earth is direct and some is diffusive. The distinction is important as while some PV systems (flat-plate systems) can use both forms of light, concentrator systems that are often more efficient can only use direct light. Optics cannot capture the diffuse light; hence, in cloudy weather conditions the efficiency of the concentrated PV system is dramatically reduced. Non-concentrated PVs accept both direct and diffuse light, but the energy produced from the direct light is significantly higher. Compared to concentrated PVs, they have higher solar cell cost due to their larger area, but save on the cost of the optics for concentration. Like in concentrated PVs, tracking systems are also often used in non-concentrating PVs to enhance the efficiency. However, in low-light or non-direct conditions like cloudy skies, non-concentrating PVs usually suffer a cutout when charge carrier mobility is low and recombination becomes a major issue. The tracker would waste energy under such conditions. A solar TE converter, on the other hand, uses the global radiation (i.e. both direct and diffuse) and has zero or very low cutout level and is more appropriate for the regions that have more cloudy weather throughout the year. Table 1 shows the calculated efficiency of the proposed cell for different weather conditions. It is seen that even in a 100% diffuse light condition, the cell is still functional. While the efficiency of a concentrated PV can be very small in a 100% cloudy sky [42] the efficiency of the solar TE converter is only about half of its efficiency in a sunny day.

The proposed solar thermoelectric cell is not intended to surpass the efficiency of the best solar cells. The main advantage of the proposed cell is that it can convert light/heat to electricity over a larger portion of the day and in diverse climates over the year. A solar cell practically generates electricity for about five hours during the day when there is sufficient sunlight. During the winter time, in cloudy weather, or in regions were direct sunlight is limited, solar cells become very inefficient. However, a solar thermoelectric cell can operate with moderate efficiency on diffusive sunlight. It should be noted that since the global radiation under these conditions is small, the produced power would also be small. Nevertheless, the solar thermoelectric cell can produce power over a longer period of time compared with concentrated PVs. This may result in lower average $/kwh per year which deserves further study.

Table 1
Efficiency of the proposed solar TE cell at different weather conditions.

Solar radiation	Cloudless blue sky	Misty, cloudy, sun visible as yellowish disc	Cloudy sky
Global radiation (W/m^2)	600–1000	200–400	50–150
Diffuse radiation (%)	10–20	20–80	80–100
Efficiency for ZT = 1 (%)	9.9–11.6	6.7–8.7	3.4–5.9
Efficiency for ZT = 3 (%)	16.8–19.2	11.8–14.9	6.4–10.6

4. Conclusion

The recent substantial progress in engineering materials with unprecedented thermoelectric (TE) efficiencies has not yet evolved into the emergence of thermoelectric devices with sizable performance improvement. Thin film TE materials with improved figure-of-merit (ZT) have been developed; however, thin film TE devices with improved efficiency are rarely reported. This can be attributed to the complexities involved in the design of a thin film thermoelectric device such as the heat management and component configuration, which greatly affect the overall efficiency. In this manuscript we described a design for a planar micro-machined thermoelectric device in which the hot junction is in the same plane as the cold junction. In this design the two major efficiency limiting factors of solar TE generators are addressed resulting in dramatic enhancement in efficiency. These factors include the ohmic contact resistance and the relative size of the IR collector area to the TE cross-section area. The application of spectrally selective coatings was further studied. It was shown that the spectrally selective coatings on the transparent cap and the substrate reflect the thermal radiation reducing the parasitic radiation heat losses. This would significantly increase the temperature of the hot junction and further enhance the efficiency. The predicted efficiency for the proposed device structure employing thermoelectric materials with ZT in the range of 1.5 is comparable with that of the state-of-the-art silicon-based photovoltaic (PV) solar cells. This makes the proposed thermoelectric solar generators a great candidate for sustainable energy generation in areas where the climate is often cloudy and direct sunlight is not available. Thermoelectric generators also benefit from longer hours of daily operation than PV cells. The execution of the proposed solar TE device structure is expected to substantially contribute to the development of a competitive technology based on highly efficient and inexpensive batch-fabricated solar thermoelectric generators.

Acknowledgment

The authors would like to thank Payam Norouzzadeh from Oklahoma State University for assistance in drawing Fig. 6(a2). This report is partially based upon work supported by Air Force Office of Scientific Research (AFOSR) High Temperature Materials program under grant no. FA9550-10-1-0010 and the National Science Foundation under grant no. 0933763.

References

[1] Lane T. Solar hot water systems: lessons learned 1977 to today. Energy Conservation Services of North Florida, Inc; 2004.
[2] Ardente F, Beccali G, Cellura M. Life cycle assessment of a solar thermal collector: sensitivity analysis, energy and environmental balances. Renew Energy 2005;30:109–30.
[3] Chiras D. The solar house: passive heating and cooling. Chelsea Green Publishing Company; 2002.
[4] Swanson RM. Photovoltaics power up. Science 2009;324.
[5] Luque A, Hegedus S. Handbook of phovoltaic science and engineering. Wiley; 2003.

[6] Mills D. Advances in solar thermal electricity technology. Sol Energy 2004;76:19–31.
[7] Forsberg CW, Peterson PF, Zhao H. J Solar Energy Eng 2007;129:141–6.
[8] Zamanipour Z, Shi X, Dehkordi AM, Krasinski JS, Vashaee D. Phys Status Solidi A 2012;209(10):2049–58.
[9] Zamanipour Z, Vashaee D. J Appl Phys 2012;112(9):093714.
[10] Satyala N, Vashaee D. Appl Phys Lett 2012;100(7):073107.
[11] Zamanipour Z, Salahinejad E, Norouzzadeh P, Krasinski JS, Tayebi L, Vashaee D. J Appl Phys 2013;114(2):023705.
[12] Snyder GJ, Toberer ES. Complex thermoelectric materials. Nat Mater 2008;7(2):105–14. http://dx.doi.org/10.1038/nmat2090.
[13] Norouzzadeh P, Myles CW, Vashaee D. J Phys Condens Matter 2013;25(47):475502.
[14] Dresselhaus M, Chen G, Ren Z, Fleurial JP, Gogna P, Tang MY, et al. MRS Proc 2007;1044(1).
[15] Vashaee D, Zhang Y, Shakouri A, Zeng G, Chiu YJ. Phys Rev B 1953;74(19):15.
[16] Vashaee D, Shakouri A. Phys Rev Lett 2012;92(10):106103.
[17] Vashaee D, Shakouri A. Microscale Thermophys Eng 2004;8(2):91–100.
[18] Lin YM, Dresselhaus MS. Phys Rev B 2003;68(7):075304.
[19] Zhang Y, Vashaee D, Christofferson J, Zeng G, LaBounty C, Piprek J, et al. In: ASME symposium on the analysis of applied heat pump and refrigeration systems; 2003. pp. 16–21.
[20] Vashaee D, LaBounty CJ, Fang X, Zeng G, Abraham P, Bowers JE, et al. Proc SPIE; 2001:139–44.
[21] Zeng G, Fan X, LaBounty C, Croke E, Zhang Y, Christofferson J, et al. Mater Res Soc Symp Proc 2004;793:43–50. paper S11.4.
[22] McEnaney K, Kraemer D, Ren Z, Chen G. J Appl Phys 2011;110:074502.
[23] Li P, Cai L, Zhai P, Tang X, Zhang Q, Niino M. J Electron Mater 2010;39(9):1522–30.
[24] Kraemer D, McEnaney K, Chiesa M, Chen G. Solar Energy; 2012:1338–50.
[25] Amatya R, Ram RJ. J Electron Mater 2010;39(9):1735–40.
[26] Kraemer D, Poudel B, Feng H, Caylor JC, Yu B, Yan X, et al. Nat Mater; 2011. http://dx.doi.org/10.1038/nmat3013.
[27] Telkes M. Solar thermoelectric generators. J Appl Phys 1954;25(6):765–77.
[28] Omer SA, Infield DG. Design optimization of thermoelectric devices for solar power generation. Solar Energy Mater Solar Cells 1998;53(1–2):67–82.
[29] Lidorenko NS, Astakhov OP, Kolomoets NV. Geliotekhnika 1984;20(3):7–9. Allerton Press, Inc.
[30] Hasan A. Review of solar thermoelectric energy conversion and analysis of a two cover flat-plate solar collector. Massachusetts Institute of Technology; 2007.
[31] Rush R. Solar flat plate thermoelectric generator research. Technical documentary report Air Force AD 605931. General Electric Corporation; 1964.
[32] Christofferson J, Vashaee D, Shakouri A, Melese P. International mechanical engineering congress exhibit; 2001.
[33] Fan X, Zeng G, LaBounty C, Vashaee D, Christofferson L, Shakouri A, et al. Twentieth international conference on thermoelectrics (Cat. No. 01TH8589), Beijing, China; 2001. pp. 405–8.
[34] Nozariasbmarz A, Tahmasbi Rad A, Zamanipour Z, Krasinski JS, Tayebi L, Vashaee D. Scr Mater 2013;69(7):549–52.
[35] Satyala N, Norouzzadeh P, Vashaee D. Nanoscale thermoelectrics. Springer International Publishing; 2014. pp. 141–83.
[36] Shi X, Zamanipour Z, Krasinski JS, Tree A, Vashaee D. An investigation of electrical contacts for higher manganese silicide. J Electron Mater 2012;41(9):2331–7.
[37] Vashaee D, Christofferson J, Zhang Y, Shakouri A, Zeng G, LaBounty Ch, et al. Microscale Thermophys Eng 2005;9:99.
[38] D. Kraemer, Master thesis, Massachusetts Institute of Technology, Cambridge, MA; 2007.
[39] Dolbier Jr WR, Beach WF. J Fluorine Chem 2003;122(1):97–104.
[40] http://windows.lbl.gov.http://www.efficientwindows.org [last accessed in 2012].
[41] Kennedy CE. Review of mid- to high-temperature solar selective absorber materials; July 2002. NREL/TP-520-31267.
[42] Solar radiation data is taken from METEONORM. Meteotest, Fabrikstrasse 14, CH-3012 Bern.